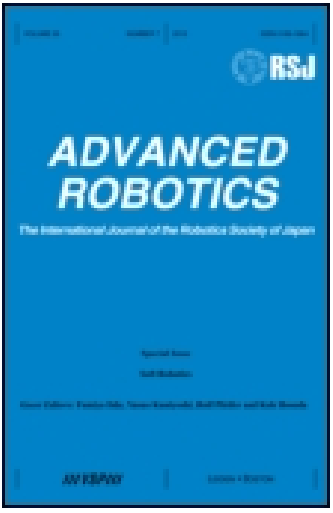

Advanced Robotics
Publication details, including instructions for authors and subscription information:
http://www.tandfonline.com/loi/tadr20

Minimum-time control of coupled tendon-driven manipulators

Shugen [a] & Mitsuru Watanabe [b]

[a] Department of Systems Engineering, Faculty of Engineering, Ibaraki University, 4-12-1 Nakanarusawa-Cho, Hitachi-Shi 316-8511, Japan

[b] Department of Systems Engineering, Faculty of Engineering, Ibaraki University, 4-12-1 Nakanarusawa-Cho, Hitachi-Shi 316-8511, Japan

Published online: 02 Apr 2012.

To cite this article: Shugen & Mitsuru Watanabe (2001) Minimum-time control of coupled tendon-driven manipulators , Advanced Robotics, 15:4, 409-427, DOI: 10.1163/156855301750398338

To link to this article: http://dx.doi.org/10.1163/156855301750398338

Advanced Robotics, Vol. 15, No. 4, pp. 409–427 (2001)

Full paper

Minimum-time control of coupled tendon-driven manipulators

SHUGEN MA * and MITSURU WATANABE

Department of Systems Engineering, Faculty of Engineering, Ibaraki University, 4-12-1 Nakanarusawa-Cho, Hitachi-Shi 316-8511, Japan

Received 4 July 2000; accepted 23 August 2000

Abstract—Hyper-redundant manipulators have very large degrees of redundancy, thus possessing unconventional features such as the ability to enter a narrow space while avoiding obstacles. In this study, a time-optimal control scheme is proposed for a hyper-redundant manipulator that was realized by coupled tendon-driven mechanisms. In the mechanisms, a pair of tendons for driving a joint is pulled from base actuators via pulleys mounted on the base-side joints and the degrees of actuation redundancy exist. The time-optimal trajectory planning problem is solved by using the phase-plane analysis and the linear programming technique. Computer simulations were also performed to show that the proposed scheme makes full use of the actuation redundancy of tendons and their coupled function to shorten motion time.

Keywords: Hyper-redundant manipulator; coupled tendon-driven mechanism; actuation redundancy; time-optimal control; traction force limit.

1. INTRODUCTION

Hyper-redundant manipulators have a very large degree of kinematic redundancy. These robots, which are analogous in design and operation to the trunk of an elephant, have unconventional features such as the ability to enter a narrow space while avoiding obstacles. However, the realization of such a hyper-redundant manipulator is difficult because there are serious engineering problems involved. One is weight, another is control of their large degrees of redundancy. A hyper-degree-of-freedom driving mechanism mounted on the arm makes the manipulator quite heavy. A powerful driving system needed to support such a long and heavy arm makes the arm even heavier. To solve the stated weight problem, the coupled tendon-driven mechanisms were thus proposed, which enable the

*E-mail: shugen@dse.ibaraki.ac.jp

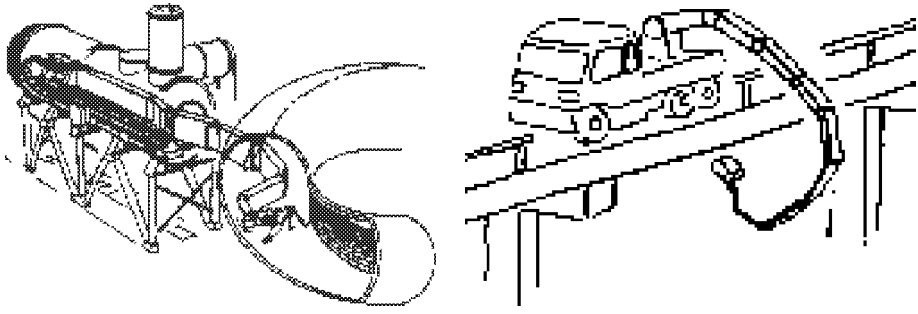

(a) (b)

Figure 1. Application examples of the planar hyper-redundant manipulator. (a) Maintenance robot for a nuclear reactor. (b) Maintenance robot a for highway.

lightweight manipulator to exhibit enormous payload capacity [1]. A hyper-redundant manipulator called the CT Arm has also been developed by using these mechanisms [2]. The developed CT Arm (see Fig. 5) has 7 d.o.f. in the vertical plane and 1 yaw d.o.f. for rotating the plane on which the manipulator arm is located to perform three-dimensional (3D) tasks. The hyper-redundancy of the CT Arm only exists in the vertical plane. The discussion of this study is thus limited to two dimensions. Even though, it is still practical for the applications as shown in Fig. 1.

To solve the control problem of the hyper degrees of freedom, an algorithm for the planar hyper-redundant manipulators where the hyper degrees of redundancy exists only in a plane, was introduced to resolve their kinematic redundancy in real-time [2–4]. The coupled tendon-driven mechanisms, except the kinematic hyper-redundancy, also have the actuation redundancy of tendons. In this study, we propose a time-optimal control scheme for the coupled tendon-driven hyper-redundant manipulators, subject to tendon traction forces due to actuator efforts. The scheme makes full use of the actuation redundancy of tendons and their coupled function. The time-optimal trajectory planning problem was solved by using the phase-plane analysis and the linear programming technique. Computer simulations were also performed to show the effectiveness of the proposed scheme.

The structure of the remainder of the paper is as follows. In Section 2, we introduce the control technique for planar hyper-redundant manipulators to resolve their kinematic hyper-redundancy. The coupled tendon-driven mechanisms of the hyper-redundant manipulator and the control technique to resolve the actuation redundancy besides the kinematic hyper-redundancy are presented in Section 3. In Section 4, we propose a time-optimal control scheme for the coupled tendon-driven hyper-redundant manipulators, subject to tendon traction forces. The computer simulations were performed to verify the validity of the proposed scheme and their results are given in Section 5. The conclusion of the paper is given in Section 6.

2. CONTROL TECHNIQUE OF HYPER-REDUNDANT MANIPULATORS

Traditionally, kinematic analysis and motion planning for kinematically redundant manipulators have relied upon a pseudoinverse [5, 6], generalized inverse [7, 8] or extended inverse [9] of the manipulator Jacobian matrix. These schemes, however, are difficult for the real-time control of hyper-redundant manipulators, because of their computational inefficiency in manipulation of the matrices. The algorithms for the position coordination of a hyper-redundant manipulator end point [2–4, 10, 11] and the algorithm for the shape control of its whole arm [12] have been introduced to resolve its kinematic redundancy. In this study, we concentrate on the discussion on the path-tracking problem and the time-optimal control.

In this section, we first introduce a real-time position coordination technique, which is based on the curvilinear theory. The time-optimal path-tracking control of the hyper-redundant manipulator in the posture space is then discussed.

2.1. Position coordination control

Curvilinear theory was used to represent the posture of kinematically hyper-redundant manipulators and to resolve their kinematic hyper-redundancy [2–4, 10, 11]. Therein, the arm posture of the hyper-redundant manipulator is modeled by a continuous curve with the curvature function $\kappa(s)$ and the torsion function $\tau(s)$, where s is the distance along the curve measured from the base. For controlling the CT Arm whose hyper-redundancy only exists in a plane, in this study we consider a curve only with curvature function $\kappa(s)$ to model the arm posture of the planar hyper-redundant manipulator. As we found, the serpenoid curve [13] better defines the arm posture of planar hyper-redundant manipulators, because the solution from the given boundary position and the length of curve to the form of curve is easily obtained.

Consider a serpeniod curve, the curvature of which is defined by:[†]

$$\kappa(s) = \frac{2\pi}{\ell} a_1 \cos\left(\frac{2\pi}{\ell} s\right) + \frac{2\pi}{\ell} a_2 \sin\left(\frac{2\pi}{\ell} s\right), \tag{1}$$

where a_1 and a_2 are the coefficients to define the curvature function, and ℓ is the curve length which is equal to the length of the manipulator arm that is to be configured. The angle $\alpha(s)$, which represents the inclination angle of the vector with respect to the x-axis on the curvilinear length s, and the end-point position $(x(\ell), y(\ell))$ can be derived and given by:

$$\alpha(s) = \alpha_0 + \int_0^s \kappa(u)\,\mathrm{d}u = \alpha_0 + a_1 \sin\frac{2\pi}{\ell} s - a_2 \cos\frac{2\pi}{\ell} s + a_2, \tag{2}$$

$$x(\ell) = \int_0^\ell \cos(\alpha(s))\,\mathrm{d}s = \cos(a_2 + \alpha_0) J_0\left(\sqrt{a_1^2 + a_2^2}\right)\ell, \tag{3}$$

[†] $\kappa(s) = A \sin((2\pi/\ell)s) + \phi)$; $A = (2\pi/\ell)\sqrt{a_1^2 + a_2^2}$, $\phi = \tan^{-1}(a_1/a_2)$.

$$y(\ell) = \int_0^{\ell} \sin(\alpha(s))\,\mathrm{d}s = \sin(a_2 + \alpha_0) J_0\left(\sqrt{a_1^2 + a_2^2}\right)\ell, \tag{4}$$

where α_0 is the initial inclination angle of the vector with respect to the x-axis at start point, and J_0 is the zero-order Bessel function [14]. While the end position of the curve is given, its form (*or posture*) corresponding to the given initial inclination angle α_0 can be defined by the coefficients a_1 and a_2.

The coefficients a_1 and a_2 are derived by solving the equations (3) and (4), and given by:

$$\begin{aligned} a_2 &= \tan^{-1}\left(\frac{y(\ell)}{x(\ell)}\right) - \alpha_0, \\ a_1 &= \left(\left[J_0^{-1}\left(\left(x(\ell)^2 + y(\ell)^2\right)^{1/2}/\ell\right)\right]^2 - a_2^2\right)^{1/2}, \end{aligned} \tag{5}$$

where J_0^{-1} is the restricted inverse zero-order Bessel function [14]. The inverse solution of the curve (*the form of the curve*) is, thus, derived and defined by the coefficients a_1 and a_2. Of course, if we change the initial inclination angle α_0, the form of the curve must be changed too, as shown in equation (2). Thus, the form of the serpenoid curve is determined by three variables a_1, a_2, α_0.

The planar hyper-redundant manipulator posture can be configured by restricting the arm onto the serpenoid curve. In this case, the joint angles are derived from the grade of the tangent line as

$$\begin{aligned} q_1 &= \alpha\left(\frac{L}{2}\right) = a_1 \sin\left(\frac{\pi}{n}\right) + a_2\left(1 - \cos\left(\frac{\pi}{n}\right)\right) + \alpha_0, \\ q_i &= \alpha\left(\left(i - 1 + \frac{1}{2}\right)L\right) - \alpha\left(\left(i - 1 - \frac{1}{2}\right)L\right) \\ &= a_1\left[\sin\left(\frac{\pi}{n}(2i-1)\right) - \sin\left(\frac{\pi}{n}(2i-3)\right)\right] \\ &\quad -a_2\left(\cos\left(\frac{\pi}{n}(2i-1)\right) - \cos\left(\frac{\pi}{n}(2i-3)\right)\right], \end{aligned} \tag{6}$$

where $i = 2, 3, \ldots, n$ (n *is the number of links of the manipulator*) and L is the length of the link, equal to ℓ/n. This discrete method through which the discrete manipulator arm (*its link length is* 0.5 *and number of links is* 7) is restricted onto the continuous serpenoid curve, makes the position error of the end position of the manipulator smaller than 10^{-6} and the position error of each joint smaller than 0.01 [15].

As a result, we know that the posture of the planar hyper-redundant manipulator is determined by three variables a_1, a_2, α_0. It should be understandable that the technique is advanced in the computational cost and makes the real-time position coordination control of planar hyper-redundant manipulators possible. It should be

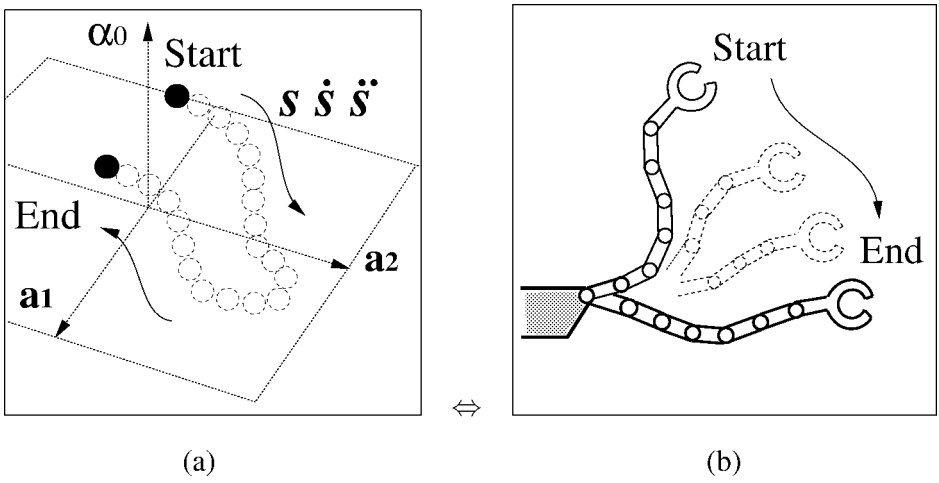

Figure 2. Mapping between the posture space (a) and the work space (b).

noted here that the introduced technique highly restricts the working area and the flexibility of hyper-redundant manipulators by constraining the manipulator arm onto the serpenoid curve. The hyper-redundant manipulator, however, is not only used in highly restricted working areas, but also must be effectively used in an open space or simply restricted space. The technique introduced in the paper is for a special case where the real-time position coordination control of the manipulator end-effector [2] and the real-time avoidance control of simple obstacles [4] are performed, and is realizable by a low-cost computer. The control system for the hyper-redundant manipulator to execute the more complicated task or preserve its high flexibility must be composed by a high-cost and high-performance computer. We will discuss this in future studies; however, it is pointed out that one method to perform the task in highly restricted areas has been proposed [2, 3] where the manipulator was divided into two parts: one passes into the narrow space (*or hole*) and another is at the outside of the hole configured by a serpenoid curve, as introduced here.

All possible postures of the planar hyper-redundant manipulator determined by a_1, a_2, α_0, defined a space that was named as the posture space, and $\lambda(a_1, a_2, \alpha_0) \in \Re^3$ was called as the posture variables [4]. As shown in Fig. 2, one of λ (shown by $\circ$ in Fig. 2) defines a posture of the arm, and the path in the posture space defines a sequence of arm postures. Comparing the end position with 2 d.o.f. with the position in the posture space, one redundancy exists (*the orientation of the manipulator end-effector can be controlled through a wrist-mounted actuator. We considered separately the position control and the orientation control of the manipulator end-effector, and in this study we only discuss the position control.*). This redundancy can be used for obstacle avoidance, torque minimization, etc. As one example, the obstacle collision-free posture space path has been generated by analysis in the

posture space [4]. Next, we discuss a problem where the manipulator traces the geometric posture space path in minimum time.

2.2. Time-optimal path-tracking control

Rewriting equation (6) in vector form, we have:

$$\boldsymbol{q}(\lambda) = \boldsymbol{\zeta}(\lambda), \tag{7}$$

where $\boldsymbol{\zeta} \in \Re^n$ is the n-dimensional vector function of the 3D vector λ. Differentiating equation (7) with respect to time, we have:

$$\begin{aligned} \dot{\boldsymbol{q}}(\lambda, \dot{\lambda}) &= \mathbf{J}_\lambda \dot{\lambda}, \\ \ddot{\boldsymbol{q}}(\lambda, \dot{\lambda}, \ddot{\lambda}) &= \mathbf{J}_\lambda \ddot{\lambda} + \dot{\mathbf{J}}_\lambda \dot{\lambda}, \end{aligned} \tag{8}$$

where $\mathbf{J}_\lambda \in \Re^{n\times 3}$ is the Jacobian matrix, with elements given by $J_{ij} = \partial \zeta_i / \partial \lambda_j$, and $\dot{\mathbf{J}}_\lambda \in \Re^{n\times 3}$ is its time-derivative, respectively.

Assume that the geometric path in the posture space is given in the parameterized form by a vector function $\boldsymbol{\eta}(s) \in \Re^3$ of the scalar path parameter $s \in \Re$, $s_0 \leqslant s \leqslant s_T$, where $\boldsymbol{\eta}(s_0)$ is the start point and $\boldsymbol{\eta}(s_T)$ is the end point of the path. Thus, we have:

$$\begin{aligned} \boldsymbol{q}(s) &= \boldsymbol{\zeta}(\boldsymbol{\eta}(s)) = \hat{\boldsymbol{\zeta}}(s), \\ \dot{\boldsymbol{q}}(s, \dot{s}) &= \mathbf{J}_\lambda \boldsymbol{\eta}' \dot{s} = \hat{\boldsymbol{J}}_s \dot{s}, \\ \ddot{\boldsymbol{q}}(s, \dot{s}, \ddot{s}) &= \mathbf{J}_\lambda \left(\boldsymbol{\eta}' \ddot{s} + \boldsymbol{\eta}'' \dot{s}^2\right) + \dot{\mathbf{J}}_\lambda \boldsymbol{\eta}' \dot{s} = \hat{\boldsymbol{J}}_s \ddot{s} + \dot{\hat{\boldsymbol{J}}}_s \dot{s}, \end{aligned} \tag{9}$$

where $\boldsymbol{\eta}'(s) = \mathrm{d}\boldsymbol{\eta}(s)/\,\mathrm{d}s \in \Re^3$, $\boldsymbol{\eta}''(s) = \mathrm{d}^2\boldsymbol{\eta}(s)/\mathrm{d}s^2 \in \Re^3$, $\hat{\boldsymbol{\zeta}}(s) = \boldsymbol{\zeta}(\boldsymbol{\eta}(s)) \in \Re^n$, $\hat{\boldsymbol{J}}_s(s) = \mathbf{J}_\lambda(\boldsymbol{\eta}(s))\boldsymbol{\eta}'(s) \in \Re^n$ and $\dot{\hat{\boldsymbol{J}}}_s(s, \dot{s}) = \mathbf{J}_\lambda(\boldsymbol{\eta}(s))\boldsymbol{\eta}''(s)\dot{s} + \dot{\mathbf{J}}_\lambda(\boldsymbol{\eta}(s), \boldsymbol{\eta}'(s)\dot{s})\boldsymbol{\eta}'(s) \in \Re^n$, respectively. As with joint angles, velocities and accelerations, the joint torques can also be represented in the parameterized form. As known, the joint torques $\tau \in \Re^n$ of the manipulator can be given in a well-known closed form:

$$\tau = \mathbf{M}_{(\boldsymbol{q})}\ddot{\boldsymbol{q}} + \boldsymbol{c}_{(\boldsymbol{q},\dot{\boldsymbol{q}})} + \boldsymbol{g}_{(\boldsymbol{q})}, \tag{10}$$

where $\mathbf{M} \in \Re^{n\times n}$ is the inertia matrix, $\boldsymbol{c} \in \Re^n$ is the torque vector of Coriolis and centrifugal forces, and $\boldsymbol{g} \in \Re^n$ is the torque vector of gravity force, respectively. Substituting equation (9) for equation (10), we have:

$$\tau(s, \dot{s}, \ddot{s}) = \boldsymbol{\mu}(s)\ddot{s} + \boldsymbol{\nu}(s, \dot{s}), \tag{11}$$

where $\boldsymbol{\mu}(s) = \mathbf{M}_{(\boldsymbol{q}(s))}\hat{\boldsymbol{J}}_s = \hat{\mathbf{M}}_{(s)}\hat{\boldsymbol{J}}_s \in \Re^n$, $\boldsymbol{\nu}(s, \dot{s}) = \hat{\mathbf{M}}_{(s)}\dot{\hat{\boldsymbol{J}}}_s\dot{s} + \hat{\boldsymbol{c}} + \hat{\boldsymbol{g}} \in \Re^n$, $\hat{\boldsymbol{c}}_{(s,\dot{s})} = \boldsymbol{c}_{(\boldsymbol{q}(s),\dot{\boldsymbol{q}}(s,\dot{s}))} \in \Re^n$ and $\hat{\boldsymbol{g}}_{(s)} = \boldsymbol{g}_{(\boldsymbol{q}(s))} \in \Re^n$. Equation (11) shows the joint torques for the hyper-redundant manipulator to track the geometric path in the posture space.

While the joint torques, τ, belong to the feasible set due to actuator efforts, Ω, defined as:

$$\Omega = \left\{\tau \,|\, \tau_{i,\min} \leqslant \tau_i \leqslant \tau_{i,\max}; i = 1, 2, \ldots, n\right\}, \tag{12}$$

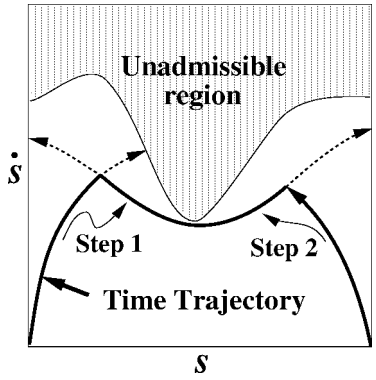

Figure 3. Generation of the path-tracking time trajectory.

the actuator-wise bounds on $\ddot{s}$ corresponding to s and $\dot{s}$ are then derived as:

$$\ddot{s}_{i,\max} = \begin{cases} (\tau_{i,\max} - \nu_i)/\mu_i & (\mu_i > 0) \\ +\infty & (\mu_i = 0) \\ (\tau_{i,\min} - \nu_i)/\mu_i & (\mu_i < 0), \end{cases}$$

$$\ddot{s}_{i,\min} = \begin{cases} (\tau_{i,\min} - \nu_i)/\mu_i & (\mu_i > 0) \\ -\infty & (\mu_i = 0) \\ (\tau_{i,\max} - \nu_i)/\mu_i & (\mu_i < 0). \end{cases}$$

The overall bounds are obtained as minimization and maximization over joints:

$$\ddot{s}_{\max} = \min_{i=1,\ldots,n} \ddot{s}_{i,\max}, \quad \ddot{s}_{\min} = \max_{i=1,\ldots,n} \ddot{s}_{i,\min}. \tag{13}$$

Note that these bounds depend on the state $[s, \dot{s}]$ and that for all admissible states the inequality $\ddot{s}_{\min} \leqslant \ddot{s}_{\max}$ must be fulfilled.

The time trajectory that describes the change of $\dot{s}$ with respect to s can be generated by the phase-plane analysis technique [16–21]. Solving the nonlinear equation $\ddot{s}_{\max}(s, \dot{s}) = \ddot{s}_{\min}(s, \dot{s})$, the maximal admissible velocities $\dot{s}_{\max}$ with respect to s were derived [21]. That is, give the displacement s and derive the velocity $\dot{s}$ with respect to s through solving $\ddot{s}_{\max}(s, \dot{s}) = \ddot{s}_{\min}(s, \dot{s})$. Further on, as shown in Fig. 3, through the recursive calculation of the path-tracking velocity accelerated by the feasible maximum acceleration from start point to end point (*Step 1*), and the recursive calculation of the path-tracking velocity decelerated by the feasible minimum acceleration backward from end point to start point (*Step 2*), the path-tracking time trajectory was generated [22]. The obtained time trajectory is a sequence of curves with maximal or minimal accelerations. The minimum time path-tracking control of hyper-redundant manipulators is performed by tracing the obtained time trajectory.

3. MECHANISM AND CONTROL OF COUPLED TENDON-DRIVEN MANIPULATORS

In this section, we introduce the coupled tendon-driven mechanisms to solve the weight problem of the hyper-redundant manipulator and the control methods specified for the mechanisms.

3.1. Mechanisms

To solve the weight problem, the coupled tendon-driven mechanisms shown in Fig. 4 have been proposed [1, 2].

3.1.1. Type 1 coupled tendon-driven mechanism. Figure 4a shows the type 1 coupled tendon-driven mechanism. It consists of free connected serial links. One pair of tendons for driving link i ($i = 1, \ldots, n$) around joint i is fixed at pulley i, which is riveted on link i while freely rotating around joint i, at one end of them; then they are wound along the way of the pulley of joints $i - 1$ through 1 in the opposite direction, to be extended to the base. In this mechanism, when generation of torque τ_i at joint i is attempted, the same torque is inevitably generated to joints 1 through $i - 1$ (*in case of uniform pulley radius*). As far as joint i is connected, power transmission pulleys to drive joints $i + 1, \ldots, n$ of the tip side are pivoted to this joint and therefore torques produced to drive these joints are accumulated at joint i. As a result, we know that the tendon traction forces are positively coupled in the mechanism to increase the payload capacity.

3.1.2. Type 2 coupled tendon-driven mechanism. Figure 4b shows the type 2 coupled tendon-driven mechanism. The basic construction of this mechanism is the same as that of the type 1. The only difference is that a pair of tendons to drive a certain joint i are passed through joints $i - 1$ to 1, where two pulleys are provided, and both tendons are stretched on the same side of the pulley. All driving tendons are designed to stretch on one side of the manipulator. The tendon-stretched side is always controlled so as to be positioned at the upper side of the

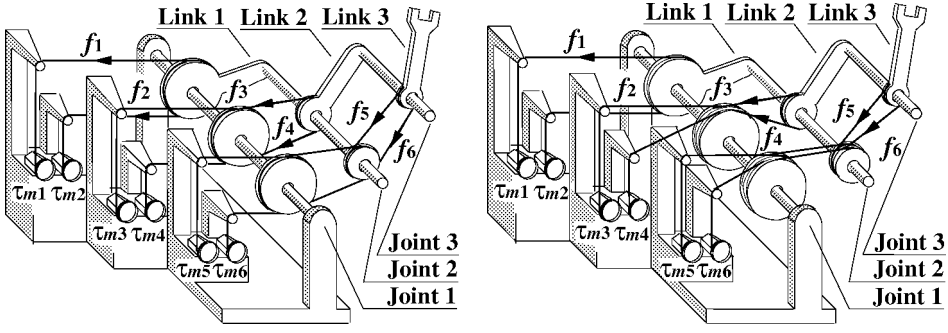

Figure 4. Coupled tendon-driven mechanisms. (a) Type 1 mechanism. (b) Type 2 mechanism.

arm with regard to gravity. The characteristics of the type 2 coupled tendon-driven mechanism is that the pair of tendons are both positively coupled to further increase the payload capacity (*in the case type 1 coupled tendon-driven mechanism, tendons are positively coupled, but only the traction difference of the pair of tendons is used to increase the payload capacity*).

Note that the simplest method for the manipulator to realize 3D motion by coupled tendon-driven mechanisms is to add a yaw motion at base of the arm and rotate the vertical plane within which the manipulator moves. The developed CT Arm has used this method to realize 3D motion. Another way for realizing 3D motion is to connect the joints in series with a torsional angle. The torsional angle must be small enough to prevent the tendon disengaging from the pulleys. This method has the property that the characteristics of the coupled tendon-driven mechanisms are not reduced.

3.2. Control technique

The control of the coupled tendon-driven mechanisms includes the tendon traction determination algorithm and the servo system to realize these tendon traction forces. In the case of driving the practical tendon-driven robot, a good servo system is necessary and lots of research has been performed on the servo system of the tendon-driven system, e.g. in [23, 24]. The tendon traction determination scheme to resolve the actuation redundancy of the tendons is to obtain the tendon traction forces through optimizing the performance criterion as the total sum of tendon traction forces.

The joint torques $\tau \in R^n$ can be expressed by the tendon traction forces $\boldsymbol{f} \in R^{2n}$ as:

$$\tau = \mathbf{D}\boldsymbol{f} \,, \tag{14}$$

where $\mathbf{D} \in R^{n\times 2n}$ is the coefficient matrix. Since the coupled tendon-driven mechanisms have n joints (*or degrees of freedom*) and each joint is driven by a pair of tendons, the number of tendons is $2n$. We let j ($j = 1 \sim 2n$) denote the tendon number from the base joint 1 to the end joint n, at the same time the upper-driving tendon is counted first and the lower-driving tendon is next for the same joint.

The matrix $\mathbf{D}$ is the matrix denoted features of the driving mechanisms; for the type 1 coupled tendon-driven mechanism, it is expressed as:

$$\mathbf{D} = \begin{bmatrix} r_1 & -r_1 & r_1 & -r_1 & \dots & r_1 & -r_1 \\ 0 & 0 & r_2 & -r_2 & \dots & r_2 & -r_2 \\ \vdots & \vdots & \vdots & \vdots & \ddots & \vdots & \vdots \\ 0 & 0 & 0 & 0 & \dots & r_n & -r_n \end{bmatrix} \in R^{n\times 2n}, \tag{15}$$

where the radius of the pulley at joint i is all assumed to be r_i; and for the type 2 mechanism, it is:

$$\mathbf{D} = \begin{bmatrix} r_1 & -r_1 & r_1 & r_1 & \dots & r_1 & r_1 \\ 0 & 0 & r_2 & -r_2 & \dots & r_2 & r_2 \\ \vdots & \vdots & \vdots & \vdots & \vdots & \ddots & \vdots \\ 0 & 0 & 0 & 0 & \dots & r_n & -r_n \end{bmatrix} \in R^{n\times 2n}, \tag{16}$$

where the same radius of the pulley is given as that of equation (15).

Generally, a tendon can generate only tension but not thrust, i.e. the value of the tendon traction forces $\boldsymbol{f}$ must be positive. In this study, it is set as:

$$\boldsymbol{f} \geqslant \boldsymbol{f}_{\min} \in R^{2n}, \tag{17}$$

$$\boldsymbol{f}_{\min} = \left[f_{1,\min} \cdots f_{j,\min} \cdots f_{2n,\min}\right]^T,$$

where $f_{j,\min}$ ($j = 1, 2, \dots, 2n$) is a positive constant that denotes the lowest value of tendon traction forces introduced to give the initial bias force.

Providing that the degrees of freedom of the end-effector of a hyper-redundant manipulator is m (*for a planar hyper-redundant manipulator, $m = 2$ or 3*), as well as the driving tendon number is $2n$ ($2n > m$), the $2n - m$ degrees of redundancy (*$n - m$ kinematic redundancy of the arm and n actuation redundancy of the tendon-driven system*) must be resolved. The kinematic redundancy can be resolved through the control technique shown in Section 2.1 or the widely-used redundancy resolution techniques [5–9] and the actuation redundancy is resolved by minimizing $\|\boldsymbol{f} - \boldsymbol{f}_0\|$ ($\boldsymbol{f}_0$: *bias force*) with constraints of equations (14) and (17) [1, 25]. However, how to make full use of the tendon traction forces to increase the path-tracking velocity or to make the coupled tendon-driven manipulators track a path in minimum time was never discussed.

4. TIME-OPTIMAL CONTROL OF COUPLED TENDON-DRIVEN MANIPULATORS

The time-optimal control problem of coupled tendon-driven manipulators is how to find a feasible time trajectory from a given geometric path (*in posture space*) with simultaneous utilization of the maximal capacities of the manipulators (*limit of tendon traction force*). How to use the actuation redundancy of the coupled tendon-driven manipulators to increase the path-tracking velocity and to make full use of the coupled function of tendons are discussed in this section.

For a n-d.o.f. manipulator, the driving tendon number is $2n$ and the n actuation redundancy exists. If we term the $\Re^n$ redundant set of tendon traction forces by $\boldsymbol{f}_c$ and the $\Re^n$ non-redundant set of tendon traction forces by $\hat{\boldsymbol{f}}_c$, the relationship

between $\boldsymbol{f}_c$ and $\hat{\boldsymbol{f}}_c$ is

$$\hat{f}_{c,k} = \begin{cases} f_{2i-1} & \text{if } f_{c,k} = f_{2i} \\ f_{2i} & \text{if } f_{c,k} = f_{2i-1}, \end{cases} \tag{18}$$

where $i = 1, 2, \ldots, n$. Therein, the total number of combinations of redundant tendons is 2^n. Rewriting equation (14) in $\boldsymbol{f}_c$ and $\hat{\boldsymbol{f}}_c$, and using equation (11), we have:

$$\boldsymbol{\mu}(s)\ddot{s} + \boldsymbol{\nu}(s, \dot{s}) = \tau = \mathbf{D}\boldsymbol{f} = \mathbf{D}_c\boldsymbol{f}_c + \hat{\mathbf{D}}_c\hat{\boldsymbol{f}}_c, \tag{19}$$

where $\mathbf{D}_c \in \Re^{n\times n}$ is the coefficient matrix corresponding to a redundant set of tendon traction forces $\boldsymbol{f}_c$, and $\hat{\mathbf{D}}_c \in \Re^{n\times n}$ is the coefficient matrix corresponding to a non-redundant set of tendon traction forces $\hat{\boldsymbol{f}}_c$. That is, if we rewrite the coefficient matrix $\mathbf{D}$ by $\mathbf{D} = [\boldsymbol{d}_1, \boldsymbol{d}_2, \ldots, \boldsymbol{d}_{2n}]$ ($\boldsymbol{d}_j \in \Re^n$), we have:

$$\mathbf{D}_c = \{\boldsymbol{d}_{c,k}\}, \quad \boldsymbol{d}_{c,k} = \begin{cases} \boldsymbol{d}_{2i-1} & \text{if } f_{c,k} = f_{2i-1} \\ \boldsymbol{d}_{2i} & \text{if } f_{c,k} = f_{2i}, \end{cases}$$

$$\hat{\mathbf{D}}_c = \left\{\hat{\boldsymbol{d}}_{c,k}\right\}, \quad \hat{\boldsymbol{d}}_{c,k} = \begin{cases} \boldsymbol{d}_{2i-1} & \text{if } \hat{f}_{c,k} = f_{2i-1} \\ \boldsymbol{d}_{2i} & \text{if } \hat{f}_{c,k} = f_{2i}. \end{cases}$$

The non-redundant set of tendon traction forces $\hat{\boldsymbol{f}}_c$, can be thus described by the redundant set of tendon traction forces $\boldsymbol{f}_c$ as:

$$\hat{\boldsymbol{f}}_c = \hat{\mathbf{D}}_c^{-1}\left(\boldsymbol{\mu}(s)\ddot{s} + \boldsymbol{\nu}(s, \dot{s}) - \mathbf{D}_c\boldsymbol{f}_c\right). \tag{20}$$

The tendon traction forces $\boldsymbol{f}$ belong to the feasible set due to actuator efforts, $\Omega_f(\Omega_c \times \hat{\Omega}_c)$, defined as:

$$\begin{aligned} \Omega_f &= \{\boldsymbol{f} \mid f_{j,\min} \leqslant f_j \leqslant f_{j,\max};\ j = 1, \ldots, 2n\}, \\ \Omega_c &= \{\boldsymbol{f}_c \mid \boldsymbol{f}_{c,\min} \leqslant \boldsymbol{f}_c \leqslant \boldsymbol{f}_{c,\max}\}, \\ \hat{\Omega}_c &= \{\hat{\boldsymbol{f}}_c \mid \hat{\boldsymbol{f}}_{c,\min} \leqslant \hat{\boldsymbol{f}}_c \leqslant \hat{\boldsymbol{f}}_{c,\max}\}. \end{aligned} \tag{21}$$

The minimum time path-tracking control problem of the coupled tendon-driven manipulators that are subject to tendon traction forces becomes: minimizing the criterion $J = \int \mathrm{d}t$, subject to $\boldsymbol{f}_{c,\min} \leqslant \boldsymbol{f}_c \leqslant \boldsymbol{f}_{c,\max}$ and $\hat{\boldsymbol{f}}_{c,\min} \leqslant \hat{\mathbf{D}}_c^{-1}(\boldsymbol{\mu}(s)\ddot{s} + \boldsymbol{\nu}(s, \dot{s}) - \mathbf{D}_c\boldsymbol{f}_c) \leqslant \hat{\boldsymbol{f}}_{c,\max}$.

4.1. Feasible path-tracking acceleration of coupled tendon-driven manipulators

The problem to obtain the feasible path-tracking acceleration of the coupled tendon-driven manipulators that are subject to tendon traction forces can be seen as a linear programming problem. The feasible path-tracking acceleration is derived by the linear programming technique, i.e. solving the linear programming problem:

$$\text{Basic variables:} \quad \boldsymbol{f}_c, \ddot{s}\ (f_{c,1}, \ldots, f_{c,n}, \ddot{s})$$

$$\text{Objective function:} \quad J = \ddot{s} - w \sum_{k=1}^{n} f_{c,k} \quad \text{(Maximization)}$$

$$J = \ddot{s} + w \sum_{k=1}^{n} f_{c,k} \quad \text{(Minimization)}$$

$$\text{Constraints:} \quad \boldsymbol{f}_{c,\min} \leqslant \boldsymbol{f}_c \leqslant \boldsymbol{f}_{c,\max}$$

$$\hat{\boldsymbol{f}}_{c,\min} \leqslant \hat{\mathbf{D}}_c^{-1}(\boldsymbol{\mu}(s)\ddot{s} + \boldsymbol{\nu}(s, \dot{s}) - \mathbf{D}_c \boldsymbol{f}_c) \leqslant \hat{\boldsymbol{f}}_{c,\max}$$

to obtain the feasible path-tracking acceleration $\ddot{s}$. The maximum value of the feasible path-tracking acceleration $\ddot{s}$, $\ddot{s}_{\max}$, is derived by maximizing the objective function $J = \ddot{s} - w \sum_{k=1}^{n} f_{c,k}$, and the minimum value of the feasible path-tracking acceleration $\ddot{s}$, $\ddot{s}_{\min}$, is derived by minimizing the objective function $J = \ddot{s} + w \sum_{k=1}^{n} f_{c,k}$. Therein, w is the weighting factor for obtaining one set of tendon traction forces. In addition to $\ddot{s}_{\max}$ and $\ddot{s}_{\min}$, the redundant set of tendon traction forces are also derived at the same time. However, since there exist redundant tendons, the tendon traction forces to generate same value of $\ddot{s}_{\max}$ or $\ddot{s}_{\min}$ may have more than one solution. Here, we utilize the minimization of the sum of redundant tendon traction forces to obtain one solution of tendon traction forces. Of course, other criteria like the minimization of the squared sum of tendon traction forces may also be used to obtain one solution from all 2^n combinations of redundant tendon traction forces $\boldsymbol{f}_c$. The non-redundant set of tendon traction forces can be derived by substituting the redundant set of tendon traction forces for equation (20). The tendon traction forces to generate $\ddot{s}_{\max}$ or $\ddot{s}_{\min}$ are thus obtained. The s and $\dot{s}$ are derived through integration. Note that for all admissible states the inequality $\ddot{s}_{\min} \leqslant \ddot{s}_{\max}$ must hold.

4.2. Generation of time trajectory

As with the time-optimal control of the common hyper-redundant manipulator that is driven by the joint-mounted actuators, the time trajectory can be generated by the phase-plane analysis technique. Solving the nonlinear equation $\ddot{s}_{\max}(s, \dot{s}) = \ddot{s}_{\min}(s, \dot{s})$, the maximal admissible velocities $\dot{s}_{\max}$ with respect to s are derived. As shown in Fig. 3, through the recursive calculation where the path is tracked by the feasible maximum acceleration from start to end (*Step 1*) and the recursive calculation where the path is tracked by the feasible minimum acceleration backward from end to start (*Step 2*), the path-tracking time trajectory can be generated [22]. The obtained time trajectory would make full use of the actuation redundancy of tendons and their coupled function.

4.3. Time-optimal control scheme specified for Type 1 mechanism

The above-stated time-optimal control scheme is possibly used for minimum time control of two types of the coupled tendon-driven mechanisms. However, seeing

the property of the type 1 mechanism, we can more simply derive the feasible path-tracking accelerations. Since the bias traction force does not affect the joint driving torque, from the coefficient matrix of the type 1 mechanism (15) we know that:

$$\begin{aligned} f_{2n-1} - f_{2n} &= \frac{\tau_n(s, \dot{s}, \ddot{s})}{r_n}, \\ f_{2i-1} - f_{2i} &= \frac{\tau_i(s, \dot{s}, \ddot{s})}{r_i} - \frac{\tau_{i+1}(s, \dot{s}, \ddot{s})}{r_{i+1}}, \\ & i = 1, 2, \ldots, n-1, \end{aligned} \tag{22}$$

and from the limits of tendon traction forces (21), we have the bound for $f_{2i-1} - f_{2i}$, given by:

$$f_{2i-1,\min} - f_{2i,\max} \leqslant f_{2i-1} - f_{2i} \leqslant f_{2i-1,\max} - f_{2i,\min}. \tag{23}$$

Substituting equations (11) and (22) for equation (23), we can obtain the $\ddot{s}$ bounds corresponding to s and $\dot{s}$ as equation (13), and is given by:

$$\ddot{s}_{\min}(s, \dot{s}) \leqslant \ddot{s}(s, \dot{s}) \leqslant \ddot{s}_{\max}(s, \dot{s}).$$

In the same way as in Section 4.2, the time trajectory for the type 1 mechanism can be generated by the phase-plane analysis technique.

5. COMPUTER SIMULATIONS

To demonstrate the effectiveness of the proposed minimum time path-tracking control scheme for the coupled tendon-driven manipulators, the computer simulations were performed on a typical personal computer (Pentium II 333 MHz). The manipulator model that we used is shown in Fig. 5, and the limit of tendon traction forces is set as $f_{\max} = 1000.0$ N and $f_{\min} = 10.0$ N. One redundant variable in the posture space, α_0, is fixed to 0.0 rad in this study. Other two variables a_1 and a_2 are directly derived from the end position of the manipulator by equation (5). While the path in the work space is given, the path in the posture space can thus be derived.

Firstly, to determine the effective performance criterion for deriving one solution of tendon traction forces from all 2^n combinations of tendons, the computer simulation was performed on the type 2 mechanism for following four cases (*for the type 1 mechanism, there only exists one solution of tendon traction forces as shown in Section 4.3. No matter what the criterion used, only one set of tendon traction forces is derived to generate feasible path-tracking acceleration. The reason is because the bias traction force does not affect the joint driving torque. Only the difference of traction forces of the pair of tendons generates the driving torque. Through setting the opposite tendon be pulled at the minimum value $f_{\min}$, the tendon traction force to give the necessary driving torque is thus easily derived by $f = f_{\min} + r\tau$*):

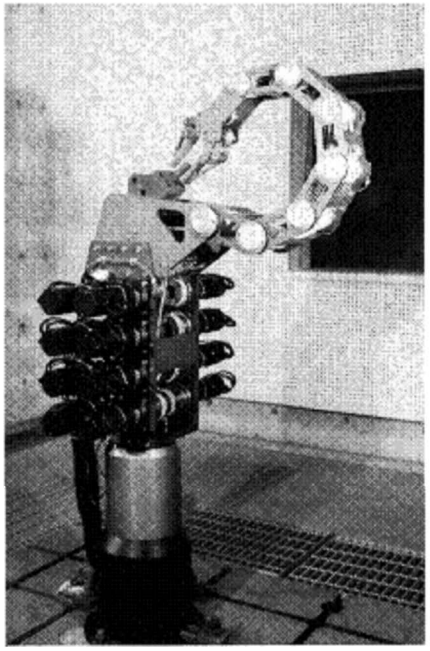

Specification of Hyper–R Arm–V

Joint	Link mass[Kg]	Joint mass[Kg]	Link length[m]	Pulley radius[m]
1	0.70	3.27	0.15	0.03
2	0.67	2.93	0.15	0.03
3	0.62	2.55	0.15	0.03
4	0.45	2.34	0.15	0.03
5	0.40	1.72	0.15	0.025
6	0.38	1.58	0.15	0.025
7	2.64	1.49	0.15	0.025

Total mass : 21.74[Kg]

Figure 5. Arm model and its parameters.

- **Case 1.** For all 2^n combinations of tendons, minimizing the squared sum of tendon traction forces, $\sum_{j=1}^{2n} f_j^2$.
- **Case 2.** For all 2^n combinations of tendons, minimizing the sum of bias forces, $\sum_{i=1}^{n} f_{\text{bias},i}$.
- **Case 3.** Assume the tendons of the upper side of the arm with regard to gravity be the redundant ones ($\boldsymbol{f}_c = [f_1, f_3, \ldots, f_{2n-1}]^T$), minimizing the sum of these tendon traction forces, $\sum_{i=1}^{n} f_{2i-1}$.
- **Case 4.** Assume the tendons of the under side of the arm with regard to gravity be the redundant ones ($\boldsymbol{f}_c = [f_2, f_4, \ldots, f_{2n}]^T$), minimizing the sum of these tendon traction forces, $\sum_{i=1}^{n} f_{2i}$.

In this simulation, the payload that we used is 20.0 kg. The path in the work space that we used is a straight line shown in Fig. 6.

Minimization of the squared sum of tendon traction forces can effectively distribute the required driving power to all tendons. The difference of the squared sum of tendon traction forces of Cases 2, 3 and 4 from Case 1 is thus listed in Table 1. For comparison, their calculation time are also given in Table 1. The reason for the large difference of the calculation time between Cases 1 and 2 and the Cases 3 and 4 is that only one time of calculation was used to derive the tendon traction forces in Cases 3 and 4, but the 2^n times of calculation are necessary in Cases 1 and 2. From Table 1, we know that, Case 1 is best to distribute the required driving power to all tendons, but takes a long calculation time. Case 3, that takes less calculation

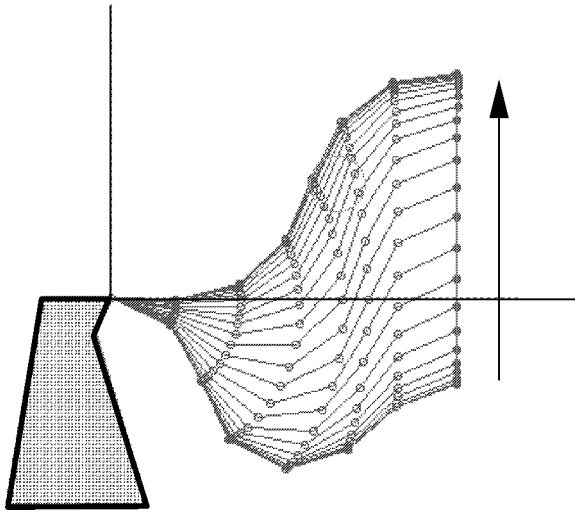

Figure 6. Arm motion and its end-point trajectory.

Table 1.
Calculation time and the difference of the squared sum of tendon traction forces for the path shown in Fig. 6

	Calculation time (s)	Difference of squared force (N^2)
Case 1	0.69	0.0
Case 2	0.69	4.28×10^4
Case 3	0.01	3.82×10^4
Case 4	0.01	5.75×10^4

time, shows the nearest value of the optimal squared sum of tendon traction forces compared with Cases 2 and 4. From the view point of the calculation time and the squared sum of tendon traction forces, we can conclude that Case 3, where the tendons of the upper side of the arm with regard to gravity are the redundant ones and the sum of these redundant tendon traction forces are minimized, is thus more effective for minimum time control of the coupled tendon-driven manipulators. In addition, the resulting motion time here is 1.063 s. For other examples, where the work space path is the circles centered at **C1**: (0.5 m, 0.0 m), **C5**: (0.9 m, 0.0 m), the radius of both being 0.1 m as shown in Fig. 7, and the payload is 10.0 kg, the same result, assuming the tendons of the upper side of the arm with regard to gravity as the redundant tendons and minimizing the sum of these redundant tendon traction forces is more effective for minimum time control of the coupled tendon-driven manipulators, was obtained, as shown in Table 2.

Next, we compare two types of coupled tendon-driven mechanisms through the time-optimal control scheme, and show how the actuation redundancy and the coupled function be effectively used. As the desired path we utilize the circles

Table 2.
Calculation time and the difference of the squared sum of tendon traction forces for paths **C1** and **C5** shown in Fig. 7

	Circle path **C1**		Circle path **C5**	
	Calculation time (s)	Difference of squared force (N^2)	Calculation time (s)	Difference of squared force (N^2)
Case 1	0.592	0.0	0.662	0.0
Case 2	0.582	9.02×10^4	0.660	8.60×10^4
Case 3	0.012	6.05×10^4	0.010	3.71×10^4
Case 4	0.010	7.83×10^4	0.012	8.31×10^4

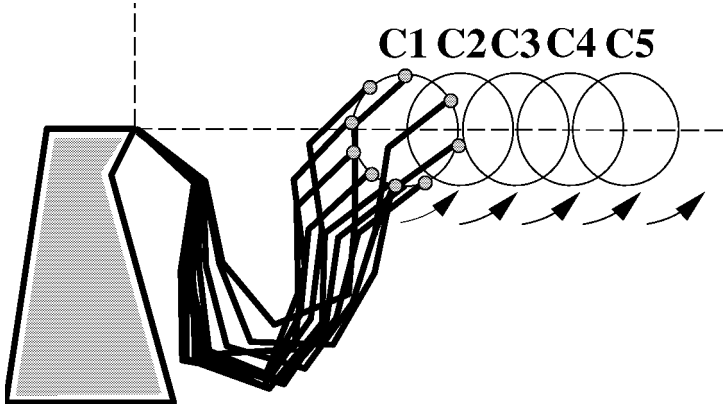

Figure 7. Circle paths in the workspace centered at **C1**: (0.5 m, 0.0 m), **C2**: (0.6 m, 0.0 m), **C3**: (0.7 m, 0.0 m), **C4**: (0.8 m, 0.0 m), **C5**: (0.9 m, 0.0 m) and their radius is 0.1 m.

centered at **C1**: (0.5 m, 0.0 m), **C2**: (0.6 m, 0.0 m), **C3**: (0.7 m, 0.0 m), **C4**: (0.8 m, 0.0 m), **C5**: (0.9 m, 0.0 m), the radius of all being 0.1 m, as shown in Fig. 7. Figure 8a shows the obtained motion time corresponding to five circle paths for two types of coupled tendon driven mechanisms, where no payload was applied ($M = 0.0$ kg). From the result, we know that while the path is near the arm base, the type 1 mechanism takes a smaller motion time than the type 2 mechanism; however, while the path is away from the arm base, the type 2 mechanism shows better performance. The reason is that, it is not yet guaranteed for the path near the arm base that the tendon-stretched side is kept at the upper side of the arm with regard to gravity in the type 2 mechanism. The type 1 mechanism becomes more effective. Using the circle path centered at **C1**: (0.5 m, 0.0 m), we compared the influence on the motion time of the payload. The result is shown in Fig. 8b. From the result, it is known that while the payload is small, the type 1 mechanism uses the less time to track the given path, however, when the payload increases, the type 2 mechanism uses a smaller motion time. At the same time, we also known that the type 2 mechanism shows good payload capacity. The reason is that, compared with the type 1 mechanism, not only the traction difference of the pair of tendons but the

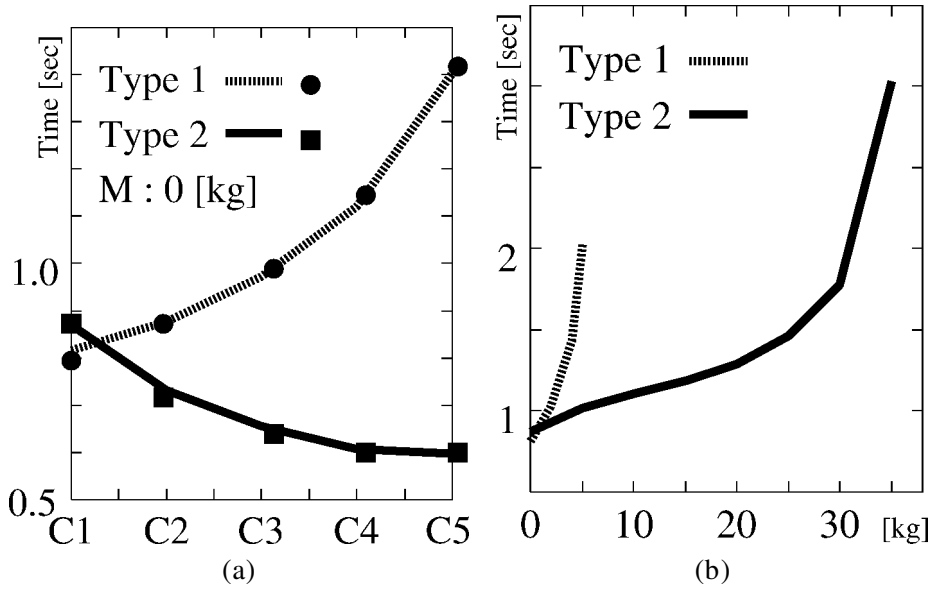

Figure 8. Comparison of the obtained optimal motion time (a) and the payload capacity (b) for two types of coupled tendon-driven mechanisms.

traction forces of the pair of tendons are both possibly used to increase the payload in the type 2 mechanism, and the proposed time-optimal control scheme has made full use of the actuation redundancy to increase the payload capacity.

6. CONCLUSIONS

In this study, a time-optimal control scheme was proposed for coupled tendon-driven manipulators, in which a pair of tendons for driving a joint is pulled from base actuators via pulleys mounted on the base-side joints and the degrees of actuation redundancy exist. The time-optimal trajectory planning problem was solved by using the phase-plane analysis and the linear programming technique. Computer simulations were also executed to show that: (i) assuming the tendons of the upper side of the arm with regard to gravity as the redundant tendons and minimizing the sum of these redundant tendon traction forces can effectively distribute the required driving power to all tendons and takes little calculation time, it is thus more effective; (ii) while the path is near the arm base or while the payload is small, the type 1 mechanism uses less time to track the given path. However, when the path is away from the arm base and the payload increases, the type 2 mechanism uses a smaller motion time. In addition, we known that the type 2 mechanism shows good payload capacity.

REFERENCES

1. S. Hirose and S. Ma, Coupled tendon-driven multijoint manipulator, in: *Proc. IEEE Int. Conf. on Robotics and Automation*, Vol. 2, pp. 1268–1275 (1991).
2. S. Ma and S. Hirose, Development of a hyper-redundant multijoint manipulator for maintenance of nuclear reactors, *Int. J. Adv. Robotics* **9** (3), 281–300 (1995).
3. G. S. Chirikjian and J. W. Burdick, An obstacle avoidance algorithm for hyper-redundant manipulators, in: *Proc. IEEE Int. Conf. on Robotics and Automation*, Vol. 1, pp. 625–631 (1990).
4. S. Ma and M. Konno, An obstacle avoidance scheme for hyper-redundant manipulators — global motion planning in posture space, in: *Proc. 1997 IEEE Int. Conf. on Robotics and Automation*, Vol. 1, pp. 161–167 (1997).
5. C. A. Klein and C. H. Huang, Review of the pseudoinverse for control of kinematically redundant manipulators, *IEEE Trans. Syst. Man Cybernet.* **13** (2), 245–250 (1983).
6. A. Liegeois, Automatic supervisory control of the configuration and behavior of multi-body mechanisms, *IEEE Trans. Syst. Man Cybernet.* **7** (12), 868–871 (1977).
7. D. N. Nenchev, Redundancy resolution through local optimization: a review, *J. Robotic Syst.* **6** (6), 769–798 (1989).
8. T. Shamir and Y. Yomdin, Repeatability of redundant manipulators: mathematical solution of the problem, *IEEE Trans. Auto. Control* **33** (11), 1004–1009 (1988).
9. J. Baillieul, Kinematic programming alternatives for redundant manipulators, in: *Proc. IEEE Int. Conf. on Robotics and Automation*, Vol. 2, pp. 1004–1009 (1985).
10. G. S. Chirikjian and J. W. Burdick, A modal approach to hyper-redundant manipulator kinematics, *IEEE Trans. Robotics Automat.* **10** (3), 343–354 (1994).
11. G. S. Chirikjian and J. W. Burdick, Kinematically optimal hyper-redundant manipulator configurations, *IEEE Trans. Robotics Automat.* **11** (6), 794–806 (1995).
12. H. Mochiyama, Shape control of manipulators with hyper degrees of freedoms, PhD thesis. Japan Advanced Institute of Science and Technology, School of Information Science (1998).
13. S. Hirose, *Biologically Inspired Robots.* Oxford University Press, Oxford (1993).
14. I. N. Sneddon, *Special Functions of Mathematical — Physics and Chemistry.* Oliver & Boyd, London (1961).
15. K. Yokoshima, Study on the control of the Moray-drive type multijoint manipulators with hyper degrees, ME dissertation. Department of Mechanical Engineering Science, Tokyo Institute of Technology (1992).
16. F. Pfeifer and R. Johanni, A concept for manipulator trajectory planning, in: *Proc. IEEE Int. Conf. on Robotics and Automation*, pp. 1399–1405 (1986).
17. J. E. Bobrow, S. Dubowsky and J. S. Gibson, Time-optimal control of robotic manipulators along specified paths, *Int. J. Robotic Res.* **4** (3), 3–17 (1985).
18. K. G. Shin and N. D. McKay, Minimum-time control of robotic manipulators with geometric path constraints, *IEEE Trans. Auto. Control.* **30** (6), 531 (1985).
19. L. Zlajpah, On time optimal path control of manipulators with bounded joint velocities and torques, in: *Proc. IEEE Int. Conf. on Robotics and Automation*, pp. 1572–1577 (1996).
20. J. Kieffer, A. J. Cahill and M. R. James, Robust and accurate time-optimal path-tracking control for robot manipulators, *IEEE Trans. Robotics Automat.* **13** (6), 880–890 (1997).
21. S. Ma, Time optimal control of manipulators with limit heat characteristics of actuator, in: *Proc. IEEE/RSJ Int. Conf. on Intelligent Robots and Systems*, pp. 318–343 (1999).
22. S. Ma, J. Zhang, I. Kobayashi and B. Cao, Time-optimal control of a moray-type robot arm with consideration of actuator's actuation characteristics, in: *Proc. Asia Control Conf.*, pp. 610–615 (2000).
23. H. Ko, C. C. Davis, E. K. Iversen and S. C. Jacobsen, High stiffness and low slew drag in an antagonistic control system, in: *Proc. IEEE Int. Conf. on Robotics and Automation*, Vol. 3, pp. 1879–1885 (1990).

24. W. T. Townsend, The effect of transmission design on force-controlled manipulator performance, PhD Thesis. Department of Mechanical Engineering, MIT (1988).
25. S. Ma, Dynamic control approach for a coupled tendon-driven manipulator, in: *Proc. 3rd Asian Conf. on Robotics and its Application*, pp. 365–370 (1997).

ABOUT THE AUTHORS

Shugen Ma was born in China in 1963. He received the BEng degree in Mechanical Engineering from Hebei Institute of Technology (Tianjin, China) in 1984. He then went on to receive his MEng and DrEng degrees in Mechanical Engineering Science from Tokyo Institute of Technology (Tokyo, Japan) in 1988 and 1991, respectively. From 1991 to 1992 he worked for Komatsu Ltd. as a Research Engineer, and from 1992 to 1993 he was at University of California (Riverside, CA) as a Visiting Scholar. Since July 1993 he has been with Ibaraki University (Japan), Faculty of Engineering. Right now he is an Associate Professor of the Department of Systems Engineering. His research interest is in the design and control theory of new types of robots, the mechanism and control of redundant manipulators, and bio-mechanics. He was awarded the outstanding paper prize from SICE in 1992. He is a member of the IEEE, JSME, SICE and the Robotics Society of Japan.

Mitsuru Watanabe was born in Japan in 1976. He received his BEng degree in Systems Engineering from Ibaraki University (Japan) in 1999. He is currently working toward the MEng degree at the Department of Systems Engineering, Ibaraki University. His research interest is in the mechanism and control of hyper-redundant manipulators. He is a student member of the Robotics Society of Japan.